

## Solubility and Stability Advantage of Aceclofenac Salts

N. Rajesh Goud, Kuthuru Suresh, and Ashwini Nangia\*

School of Chemistry, University of Hyderabad, Prof. C. R. Rao Road, Gachibowli, Central University P.O., Hyderabad 500 046, India

## Supporting Information

**ABSTRACT:** The nonsteroidal anti-inflammatory drug aceclofenac was screened with pharmaceutically acceptable cofomers to discover novel solid forms of improved solubility. First, the X-ray crystal structure of aceclofenac (ACF) was analyzed to contain the rare carboxylic acid catemer O–H...O synthon, stabilized by auxiliary C–H...O and Cl...O interactions. Slurry grinding of aceclofenac with different cofomers in a fixed stoichiometry resulted in salts with cytosine (1:1), piperazine (1:0.5), L-lysine (1:1), and  $\gamma$ -aminobutyric acid (1:1). The problem of drug cyclization to give the inactive indolinone byproduct is avoided in the mild conditions of salt formation. All the salts were characterized by spectroscopic methods, thermal analysis, and X-ray diffraction. Aceclofenac-L-lysine salt showed 135 times faster intrinsic dissolution rate (IDR) and 127 times higher area under the curve (AUC) compared to aceclofenac. ACF-LYS is a high solubility salt that is stable in the accelerated International Conference on Harmonization (ICH) conditions of 40 °C and 75% relative humidity for 8 months.



## INTRODUCTION

The modification of solid-state properties of a drug molecule through polymorph, salt, cocrystal etc. can significantly modulate its solubility, dissolution, and bioavailability.<sup>1</sup> Whereas solubility modulation through cocrystallization<sup>2</sup> has received considerable attention in the past decade, salt formation is the traditional and widely accepted technology for improving the solubility, solid form stability, and filterability of solid dosage forms. Moreover, salt formation is the preferred approach for aqueous solubility enhancement of liquid formulations of a drug for parenteral administration.<sup>3</sup> A current challenge in the pharmaceutical industry is to improve the physicochemical properties of poorly soluble drugs without changing their chemical structure.<sup>2b,4</sup>

Aceclofenac (2-(2,6-dichlorophenylamine)-phenylacetoxycetic acid, ACF hereafter) is an orally effective nonsteroidal anti-inflammatory drug (NSAID) with remarkable anti-inflammatory, analgesic, and antipyretic properties.<sup>5</sup> It belongs to the class of phenyl acetic acid derivatives and was found to be the most tolerated drug among NSAIDs with a lower incidence of adverse gastrointestinal effects. ACF is a BCS class II drug with poor aqueous solubility of 58  $\mu\text{g}/\text{mL}$ .<sup>6</sup> The solubility of ACF has been improved by making a triethanolamine salt<sup>7</sup> and arginate salt<sup>8</sup> as well as solid dispersion techniques.<sup>9</sup> A pharmaceutical cocrystal of ACF with nicotinamide was recently reported<sup>10</sup> and characterized by FT-IR and differential scanning calorimetry (DSC). However no solubility and dissolution information on the cocrystal is known in the literature. Other reports describe the formation of ACF derivatives<sup>11</sup> and solid form stability of salts in water.<sup>12</sup> Very few reports on the solid forms of ACF, especially salts, is discussed perhaps due to its degradation in strongly acidic or

basic conditions to give the inactive indolinone byproduct<sup>12,13</sup> (Scheme 1).

The cyclized product (indolinone) was also isolated during our attempts to form the sodium or potassium salt of ACF with bases such as  $\text{Na}_2\text{CO}_3$ ,  $\text{NaOH}$ ,  $\text{KOH}$ ,  $\text{K}_2\text{CO}_3$ , etc. The ORTEP diagram of the cyclized product is shown in Figure S1 (Supporting Information). Therefore, unlike the other members of its class, such as indomethacin and diclofenac, which are marketed as their sodium salt trihydrate and potassium salt respectively, ACF is marketed as a neutral drug.

A systematic study of ACF using crystal engineering<sup>14</sup> principles has not been reported in the literature. This is surprising because the supramolecular synthon<sup>15</sup> strategy would offer diverse options for solubility modulation of such chemically labile drug molecules. Hence we set out to address the poor solubility of ACF by developing cocrystals and salts based primarily on the robustness of functional groups and acid constants ( $\text{pK}_a$ ) of the cofomers.<sup>2,16</sup> The ability of the COOH group in ACF to assemble cocrystals with complementary functional groups such as carboxamide, pyridine, etc. through the corresponding heterosynthon<sup>17</sup> is well documented for pharmaceutical cocrystals. In this background, mechanochemical and slurry grinding<sup>18</sup> of ACF with selective GRAS cofomers<sup>19</sup> was carried out, and the products were characterized for cocrystal/salt/hydrate formation.

We report salts of ACF with piperazine (PIP), cytosine (CYT), L-lysine (LYS), and  $\gamma$ -aminobutyric acid (GABA) (see Scheme 2). A salt hydrate with piperazine and a cocrystal

Received: December 13, 2012

Revised: February 19, 2013

Published: February 21, 2013



Table 2. Crystallographic Parameters of ACF Salts

	ACF	ACF–BIP–H <sub>2</sub> O (1:0.5:0.5)	ACF–CYT (1:1)	ACF–PIP (1:0.5)	ACF–PIP–H <sub>2</sub> O (1:0.5:1)
emp form	C <sub>16</sub> H <sub>13</sub> Cl <sub>2</sub> NO <sub>4</sub>	C <sub>42</sub> H <sub>36</sub> C <sub>14</sub> N <sub>4</sub> O <sub>9</sub>	C <sub>20</sub> H <sub>18</sub> Cl <sub>2</sub> N <sub>4</sub> O <sub>5</sub>	C <sub>18</sub> H <sub>18</sub> Cl <sub>2</sub> N <sub>2</sub> O <sub>4</sub>	C <sub>18</sub> H <sub>20</sub> Cl <sub>2</sub> N <sub>2</sub> O <sub>5</sub>
form wt	354.17	882.55	465.28	397.24	415.26
cryst syst	monoclinic	monoclinic	monoclinic	monoclinic	monoclinic
sp gr	<i>P</i> <sub>2</sub> <sub>1</sub> / <i>n</i>	<i>P</i> <sub>2</sub> <sub>1</sub> / <i>c</i>	<i>P</i> <sub>2</sub> <sub>1</sub> / <i>n</i>	<i>P</i> <sub>2</sub> <sub>1</sub> / <i>n</i>	<i>P</i> <sub>2</sub> <sub>1</sub> / <i>c</i>
<i>T</i> (K)	100(2)	100(2)	100(2)	100(2)	100(2)
<i>a</i> (Å)	12.284(3)	7.5085(5)	11.2960(10)	9.1898(11)	14.555(4)
<i>b</i> (Å)	8.198(2)	11.9908(8)	8.7429(8)	5.5983(7)	14.950(4)
<i>c</i> (Å)	15.484(4)	22.2488(15)	20.8507(19)	34.890(4)	8.557(3)
$\alpha$ (°)	90	90	90	90	90
$\beta$ (°)	96.174(4)	91.5690(10)	98.0120(10)	94.038(2)	92.473(4)
$\gamma$ (°)	90	90	90	90	90
<i>Z</i>	4	2	4	4	4
<i>V</i> (Å <sup>3</sup> )	1550.3(7)	2002.4(2)	2039.1(3)	1790.5(4)	1860.1(9)
rfins collect	15306	18720	20400	17574	18911
unique rfins	3030	3520	4019	3515	3674
obsd rfins	2305	3315	3791	3143	3504
parameters	216	288	300	247	264
<i>R</i> <sub>1</sub>	0.0535	0.0293	0.0361	0.0499	0.0335
w <i>R</i> <sub>2</sub>	0.1288	0.0770	0.0880	0.1112	0.0825
GOF	1.047	1.056	1.102	1.130	1.103

**Aceclofenac–4,4′-Bipyridine–Hydrate (ACF–BIP–HYD).** Crystallization of ACF and BIP in a 1:0.5 stoichiometry in a MeOH–CH<sub>3</sub>CN solvent mixture afforded single crystals of ACF–BIP hydrate which solved and refined in the monoclinic space group *P*<sub>2</sub><sub>1</sub>/*c* in a 1:0.5:0.5 ratio. The water O atom was refined with s.o.f. of 0.5 (Figure S3b). The most acidic COOH donor in ACF is hydrogen bonded to the most basic pyridine N acceptor of BIP through an O–H···N hydrogen bond (O1···N2, 1.62 Å, 172°) (Figure 2a), consistent with Etter's hydrogen bond pairing rules.<sup>27</sup> ACF molecules in adjacent layers are connected through water molecules acting as bridges (O5–H5A···O2, 1.81 Å, 181°, and O5–H5B···O2, 1.88 Å, 151°) (Figure 2b). Auxiliary Cl···O interactions provide support to the crystal structure.

**Cytosinium–Aceclofenate Salt (ACF–CYT).** Single crystals of 1:1 cytosinium aceclofenate salt were obtained from EtOH–CH<sub>3</sub>CN. The X-ray crystal structure of ACF–CYT was solved and refined in space group *P*<sub>2</sub><sub>1</sub>/*n* (Table 1, see ORTEP in Figure S3c). The major difference between this crystal structure and that of ACF–BIP–HYD is that the proton is transferred from the COOH group of ACF to the basic N2 nitrogen of CYT via an ionic N2–H1A<sup>+</sup>···O1<sup>−</sup> hydrogen bond (1.71 Å, 180°) resulting in a salt. The protonation state of the carboxylic acid and the basic nitrogen in acid–base structures can be difficult to predict in multicomponent structures. There are several cases of borderline proton location and a continuum of O···H···N hydrogen bond states have been noted.<sup>28</sup> The electron density maps of X-ray diffraction showed that the acidic H atom is transferred and covalently bonded to the cytosine N, making a hydrogen bond with the COO<sup>−</sup> acceptor. The two C–O distances are near equal (1.246(2) Å, 1.267(2) Å) in the carboxylate group. Hydrogen bonding is mediated by the two-point carboxylate···aminopyrimidine synthon of *R*<sub>2</sub><sup>2</sup>(8) geometry. Two ACF molecules are hydrogen-bonded to two CYT molecules via the carboxylate···amine *R*<sub>2</sub><sup>4</sup>(8) motif. The N3 nitrogen of CYT forms a N3–H3A···O1 hydrogen bond with the O1 carboxylate oxygen (1.74 Å, 173°) of ACF (Figure 3).

**Piperazinium–Aceclofenate Salt (ACF–PIP).** This molecular salt crystallized in space group *P*<sub>2</sub><sub>1</sub>/*n* with one molecule of aceclofenate anion and a half molecule of piperazinium cation in the asymmetric unit (Figure S3d). The piperazinium cation forms two N<sup>+</sup>–H···O<sup>−</sup> ionic hydrogen bonds, N2<sup>+</sup>–H1A···O1<sup>−</sup> (1.68 Å, 169°) and N2<sup>+</sup>–H1A···O2<sup>−</sup> (2.46 Å, 124°). C–O bond distances and C–N–C bond angles are consistent with those for a salt species<sup>20</sup> (Figure 4). Piperazine is a pharmaceutically acceptable cyclic diamine with anthelmintic activity. Given its high basicity (p*K*<sub>a</sub> = 9.72), it can act both as a neutral and a cationic cofomer to give a cocrystal or a salt depending on the acidity of the parent API. Three monocationic forms of piperazine with anti-inflammatory drug meclofenamic acid were reported from our group.<sup>29</sup> In this work two dicationic forms of piperazine, ACF–PIP and ACF–PIP–HYD, are added.

**Piperazinium–Aceclofenate Monohydrate Salt (ACF–PIP–HYD).** This 1:0.5:1 salt hydrate crystal obtained from EtOH–CH<sub>3</sub>CN (Figure S3e) was solved in space group *P*<sub>2</sub><sub>1</sub>/*c*. One side of the dicationic piperazinium molecule is connected to aceclofenate anion through N<sup>+</sup>–H···O<sup>−</sup> ionic hydrogen bond, N2<sup>+</sup>–H1A···O1<sup>−</sup> (1.67 Å, 175°), and on the other side ACF and water molecules bridge through N2<sup>+</sup>–H2C···O5 (1.84 Å, 144°) and O5–H5B···O1<sup>−</sup> (1.83 Å, 171°) hydrogen bonds respectively, resulting in a *R*<sub>4</sub><sup>6</sup>(12) ring motif (Figure 5).

Crystal structural analysis gave an idea of the packing efficiency and bond strength of ACF salts compared to the neutral molecule. As discussed earlier, ACF can form major bonding interactions through its ester, amine, and acid functional groups. Structural analysis showed that the N–H and ester functional groups are held together by an intramolecular hydrogen bond in ACF and its solid forms. Therefore, the homomeric and heteromeric interactions in ACF and its solid forms are primarily due to the hydrogen bonding interactions at the COOH functional group. In ACF, the acid protons form a catemeric O1–H1A···O2 interaction (1.90 Å) with a neighboring molecule stabilized by auxiliary C–H···O interactions (Figure 1). In ACF–BIP–HYD, a heteromeric O1–H1A···N2 hydrogen bond (1.62 Å) with

Table 3. Hydrogen Bond Distances and Angles in ACF and Salts (N–H, O–H, and C–H Distances Were Neutron-Normalized)

D–H...A	D...A (Å)	H...A (Å)	D–H...A (deg)	symmetry code
ACF				
O1–H1A...O2	2.690(3)	1.90	135	$3/2 - x, -1/2 + y, 1/2 - z$
N1–H1B...Cl1	2.968(3)	2.63	100	<i>a</i>
N1–H1B...O4	3.025(3)	2.13	147	<i>a</i>
C2–H2A...O4	3.397(4)	2.32	171	$1 - x, -y, -z$
C4–H4B...O2	3.366(3)	2.29	174	$3/2 - x, 1/2 + y, 1/2 - z$
ACF–BIP–H <sub>2</sub> O (1:1:0.5)				
O1–H1A...N2	2.5970(16)	1.63	173	$2 - x, -1/2 + y, 1/2 - z$
N1–H1B...Cl1	2.9726(12)	2.55	113	<i>a</i>
N1–H1B...O4	3.0095(16)	2.28	148	<i>a</i>
O5–H5A...O2	2.794(3)	1.81	168	$1 - x, 1/2 + y, 1/2 - z$
O5–H5B...O2	2.786(3)	1.88	151	$-1 + x, 1/2 - y, -1/2 + z$
C4–H4A...O5	3.097(3)	2.48	121	$1 - x, -1/2 + y, 1/2 - z$
ACF–CYT (1:1)				
N2–H1A...O1	2.7150(19)	1.71	180	$1 - x, 2 - y, -z$
N1–H1B...Cl1	3.0163(15)	2.63	103	<i>a</i>
N1–H1B...O3	2.9175(19)	2.04	144	<i>a</i>
N3–H3A...O1	2.7420(18)	1.74	173	$1/2 + x, 3/2 - y, 1/2 + z$
N4–H4C...O2	2.857(2)	1.85	178	$1 - x, 2 - y, -z$
N4–H4D...O2	2.7902(19)	1.93	141	<i>a</i>
C4–H4B...O2	3.521(2)	2.44	174	$1 - x, 2 - y, -z$
C14–H14...O5	3.213(2)	2.43	128	$-1 + x, y, z$
ACF–PIP (1:0.5)				
N2–H1A...O1	2.673(3)	1.68	169	$x, 1 + y, z$
N2–H1A...O2	3.142(3)	2.46	124	$x, 1 + y, z$
N1–H1B...Cl1	3.013(2)	2.62	103	<i>a</i>
N1–H1B...O3	2.924(3)	2.04	145	<i>a</i>
N2–H2C...O2	2.653(3)	1.65	173	$x, 1 + y, z$
C2–H2A...O1	3.497(3)	2.44	164	$x, -1 + y, z$
C4–H4A...Cl1	3.510(3)	2.64	137	$x, 1 + y, z$
ACF–PIP–H <sub>2</sub> O (1:0.5:1)				
N2–H1A...O1	2.6792(19)	1.67	175	$-x, -y, 1 - z$
N1–H1B...Cl2	2.9949(17)	2.60	103	<i>a</i>
N1–H1B...O4	2.970(2)	2.12	141	<i>a</i>
N2–H2C...O5	2.724(2)	1.84	144	<i>a</i>
O5–H5A...O2	2.7106(19)	1.73	178	$x, 1/2 - y, 1/2 + z$
O5–H5B...O1	2.8090(19)	1.83	171	$x, 1 + y, 1 + z$
C2–H2B...O4	2.693(2)	2.26	102	<i>a</i>
C2–H2B...O3	3.446(2)	2.47	150	$x, -1/2 - y, -1/2 + z$
C4–H4A...O1	3.561(2)	2.51	163	$x, -1/2 - y, 1/2 + z$
C17–H17B...O2	3.231(2)	2.32	140	$x, 1 + y, z$
C18–H18A...O4	3.222(2)	2.38	134	$x, 1/2 - y, 1/2 + z$

<sup>a</sup>Intramolecular hydrogen bond.

BIP is observed. The layered motif of ACF molecules in ACF–BIP–HYD is further stabilized by water bridges. The complete transfer of acidic proton to the basic nitrogen resulted in a short and ionic bond in the salt structures. Apart from the bifurcated N–H...O<sup>−</sup> interactions (1.68 Å in ACF–PIP and 1.67 Å in ACF–PIP–HYD), a two point R<sub>2</sub><sup>2</sup>(8) ring motif between carboxylate and aminopyrimidine moieties strengthens the crystal structure of ACF–CYT. Therefore all the solid forms of ACF are stabilized by stronger and shorter ionic interactions which will impart improved physicochemical properties. This latter point is confirmed in our solubility and solid form stability studies of ACF salts (discussed later) where the salts (except ACF–PIP) were found to be stable in accelerated International Conference on Harmonization (ICH) conditions and positively modulated the solubility of the parent drug.

**Conformational Flexibility.** The chemical diagram of ACF (Scheme 2) suggests that this conformationally flexible molecule (rotation at C–N and CH<sub>2</sub>–COO moieties) can adopt different conformations in the solid-state. Significant differences were observed in the conformations of ACF in its guest free form and salt/cocrystal structures. The different conformations due to free rotation about single bonds,<sup>30</sup> mainly the acetoxyacetic acid group, are shown in Figure 6. Selected torsional angles are listed in Table S1.

**Powder X-ray Diffraction.** PXRD<sup>31</sup> is a reliable characterization tool to establish the formation of novel solid forms. It can unambiguously distinguish the resulting product phases from its starting materials through the unique diffraction line pattern. The PXRD of the novel solid forms prepared in this work (Figure S4) confirm the bulk solid phase purity and homogeneity of each crystalline phase which showed an

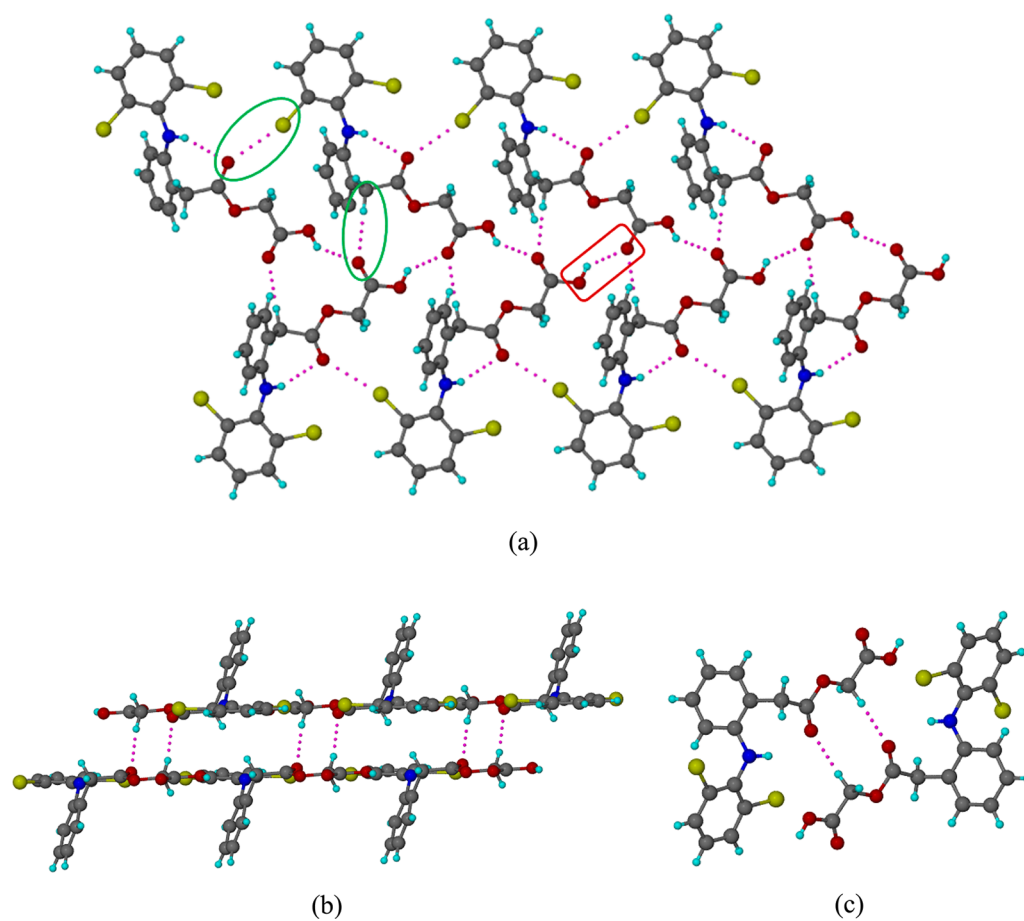


**Figure 1.** (a) Catemeric O–H...O hydrogen bonds extend the ACF molecules in a tape motif supported by auxiliary C–H...O and Cl...O interactions. The strong O–H...O H bond is marked by a rectangle (red) and the weak C–H...O and Cl...O interactions by a circle (green). (b) Weak C–H...O's connecting the adjacent catemer tapes. (c) Molecules in adjacent layers are connected through by a centrosymmetric C–H...O  $R_2^2(10)$  motif.

excellent overlay of the experimental powder pattern with the calculated lines from the crystal structure. ACF–LYS and ACF–GABA were compared with the starting components to establish novel product phases. Their single crystal X-ray structures are not available for comparison.

**Thermal Analysis.** The DSC of cocrystal/salt showed a unique melting point compared to that of the starting components; a TGA trace established the stoichiometry of water or solvent in the case of hydrates and solvates. The thermal measurements complement the XRD patterns to confirm the formation of the novel crystalline forms. The characteristic melting/decomposition profiles are shown as endo-/exotherm in the DSC heating curve. The DSC trace of each novel solid form prepared in this work (Figure 7) showed a unique melting behavior which distinguishes it from the starting materials. We did not notice any correlation between the melting point of the coformer and its corresponding salt, similar to recent cocrystal systems<sup>15a,16</sup> (Table 4). The water stoichiometry in ACF–BIP–0.5HYD and ACF–PIP–HYD bulk phases was confirmed by TGA and HSM experiments (Figure S5), which showed an excellent match with the calculated amount of water in the crystal structure.

**Vibrational Spectroscopy.** Changes in the hydrogen bonding patterns of the starting materials on forming cocrystals/salts are expected to influence the energies of vibrational modes associated with the functional groups.<sup>32</sup>

Changes in the bonding patterns hint at the functional groups involved and efficiently complement the diffraction methods for the characterization of solid-state forms. In the IR spectrum of ACF, the COOH functional group is present as a monomer, and hence the carbonyl group appears as a sharp peak at  $1771.4\text{ cm}^{-1}$ . The ester and amine functional moieties are connected to each other through intramolecular hydrogen bonds and appear at  $1716.6\text{ cm}^{-1}$  and  $3318.9\text{ cm}^{-1}$ . The bands due to C–O stretch and O–H bend appear at  $1256.4\text{ cm}^{-1}$  and  $1400.0\text{ cm}^{-1}$ . These hydrogen bonding functional groups showed significant changes in their vibrational modes on salt/cocrystal formation (Figure S6). In ACF–BIP–HYD, the N–H stretching frequency shifted to  $3296.2\text{ cm}^{-1}$ , and its bending frequency appeared at  $1602.2\text{ cm}^{-1}$ . Due to its hydrogen bonding to the acid moiety of ACF, the C=N stretch in BIP shifted from  $1408.5\text{ cm}^{-1}$  to  $1416.9\text{ cm}^{-1}$  in the cocrystal. The acid moiety exists as a carboxylate anion in all salts, characterized by the strong asymmetric stretch at  $1650\text{--}1450\text{ cm}^{-1}$ , and a weaker symmetric stretch near  $1350\text{--}1250\text{ cm}^{-1}$  in their IR spectra. The asymmetric and symmetric stretching frequencies of carboxylate salt appear at  $1492.2\text{ cm}^{-1}$  and  $1232.4\text{ cm}^{-1}$  in ACF–CYT,  $1450.8\text{ cm}^{-1}$ , and  $1245.6\text{ cm}^{-1}$  in ACF–PIP,  $1453.7\text{ cm}^{-1}$  and  $1292.5\text{ cm}^{-1}$  in ACF–PIP–HYD,  $1453.3\text{ cm}^{-1}$  and  $1242.1\text{ cm}^{-1}$  in ACF–LYS, and  $1452.1\text{ cm}^{-1}$  and  $1241.1\text{ cm}^{-1}$  in ACF–GABA as compared to the  $1771.4\text{ cm}^{-1}$  stretching peak of carboxylic acid in ACF. The Raman

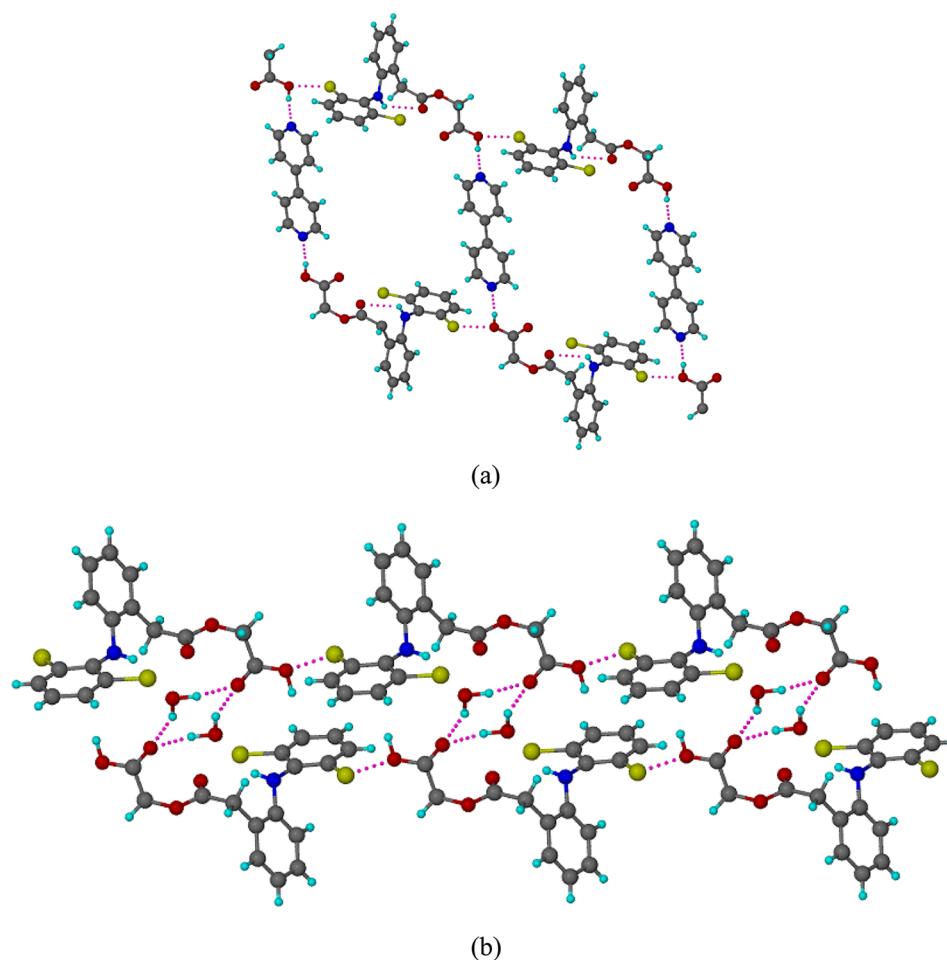


**Figure 2.** (a) ACF and BIP molecules are connected through O–H...N hydrogen bond. (b) Adjacent ACF layers are connected through water bridges in a tetramer O–H...O motif.

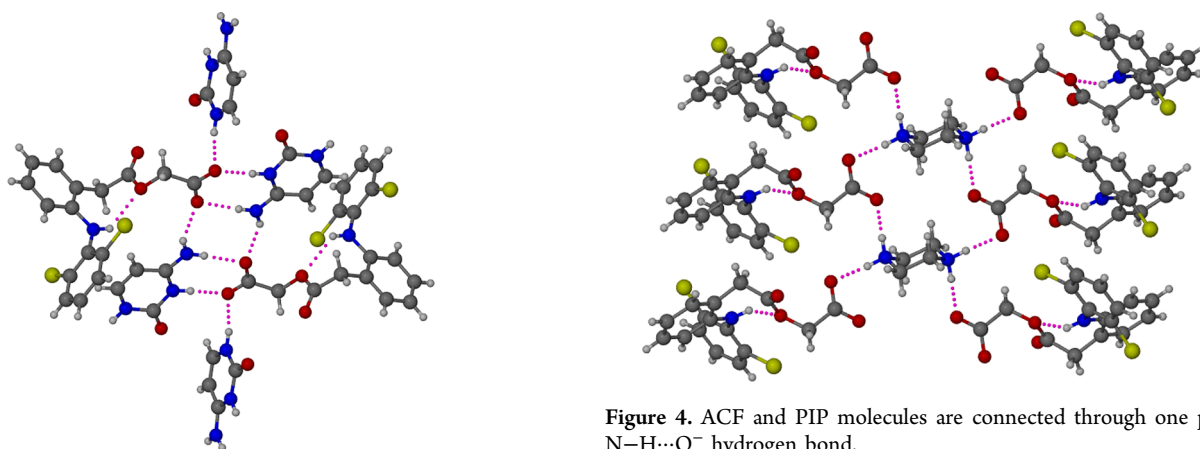


**Figure 3.**  $R_2^2(8)$  and  $R_2^4(8)$  N–H...O hydrogen bond ring motifs in the crystal structure of ACF–CYT salt.

spectra also showed similar changes in the product phases compared to the starting components (Figure S7). In ACF–BIP–HYD, the Raman shift for N–H stretching frequency was observed at  $3299.7\text{ cm}^{-1}$ , and its bending frequency at  $1611.5\text{ cm}^{-1}$  indicating changes in hydrogen bonding. The Raman asymmetric and symmetric stretching frequencies of the carboxylate group appeared at  $1414.2\text{ cm}^{-1}$ ,  $1254.9\text{ cm}^{-1}$  in ACF–CYT,  $1450.8\text{ cm}^{-1}$ ,  $1237.0\text{ cm}^{-1}$  in ACF–PIP,  $1451.7$

**Figure 4.** ACF and PIP molecules are connected through one point N–H...O<sup>−</sup> hydrogen bond.

$\text{cm}^{-1}$ ,  $1237.0\text{ cm}^{-1}$  in ACF–PIP–HYD,  $1425.2\text{ cm}^{-1}$ ,  $1234.7\text{ cm}^{-1}$  in ACF–LYS, and  $1420.9\text{ cm}^{-1}$ ,  $1234.2\text{ cm}^{-1}$  in ACF–GABA compared to the monomeric carboxylic acid peak at  $1726.4\text{ cm}^{-1}$  for ACF. Thus both IR and Raman spectra of cocrystal and salts exhibited significant differences in their stretching and bending frequencies (Tables S2 and S3) which established their unique intermolecular bonding pattern. They complement the diffraction techniques to confirm the novelty of salts.

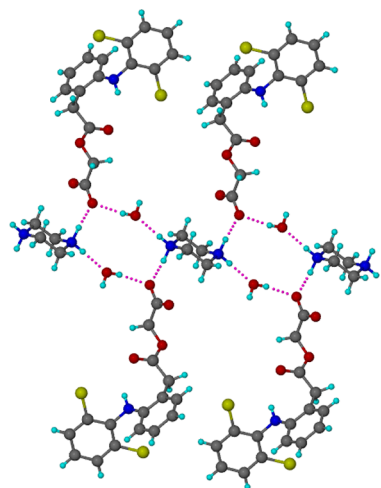


**Figure 5.**  $R_4^6(12)$  hydrogen bond ring motif in the crystal structure of ACF-PIP-HYD salt hydrate.

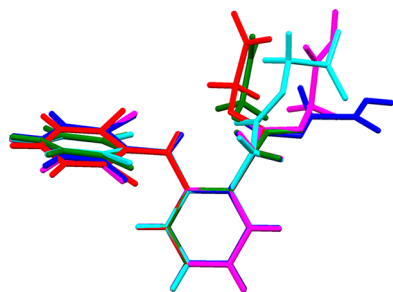


**Figure 6.** An overlay diagram of the ACF molecule extracted from the guest free form and salts. Color codes: violet = ACF, magenta = ACF-BIP-HYD, green = ACF-CYT, red = ACF-PIP, and blue = ACF-PIP-HYD.

**ss-NMR Spectroscopy.** ss-NMR spectroscopy can non-destructively provide detailed information about the differences in hydrogen bonding, molecular environment, and short-range

**Table 4.** Melting Point of ACF Salts/Cocrystals and the Coformers<sup>a</sup>

s. no.	ACF salts/cocrystal	melting point (°C)	coformer	melting point (°C)
1	ACF-BIP-HYD	132.4	4,4'-bipyridine	110–114
2	ACF-CYT	185.2	cytosine	320–325
3	ACF-PIP	164.2	piperazine	106
4	ACF-PIP-HYD	166.2	piperazine	106
5	ACF-LYS	201.0	L-lysine	196
6	ACF-GABA	135.5	$\gamma$ -aminobutyric acid	203

<sup>a</sup>Melting point of ACF 151.4 °C.<sup>21</sup>

order in crystalline and amorphous solids.<sup>33</sup> <sup>13</sup>C ss-NMR analysis of the novel solid forms of ACF showed clear differences in the product phases when compared with the starting components. On the basis of the extent of proton transfer, the position of the COOH carbon atom differed in ss-NMR spectra. Whereas the neutral COOH peak appeared at 174.1 ppm in the parent drug, it showed a clear downfield shift in salts where it exists as a carboxylate anion (Figure S8). In ACF-BIP-HYD, there is no proton transfer from ACF to the coformer. Hydrogen bonding of the COOH donor to the pyridyl nitrogen of BIP showed a downfield shift to 174.8 ppm. In salts, larger downfield shifts were observed due to complete proton transfer. The chemical shift of COO<sup>-</sup> carbon in salts was shifted downfield to 176.5 ppm in ACF-CYT, 174.4 in ACF-PIP, 174.8 in ACF-PIP-HYD, 175.1 ppm in ACF-LYS, and 174.9 ppm in ACF-GABA (Table S4).

**Solid Form Stability.** Solid form stability of salts was measured under accelerated stability ICH<sup>34</sup> conditions of 40 °C and 75% relative humidity (RH). PXRD was recorded on all the solid forms at monthly intervals for up to 8 months. ACF-CYT, ACF-PIP-HYD, ACF-LYS, and ACF-GABA were found to be as stable as the reference drug ACF in the 8 months period by PXRD. The final PXRD patterns of the solids

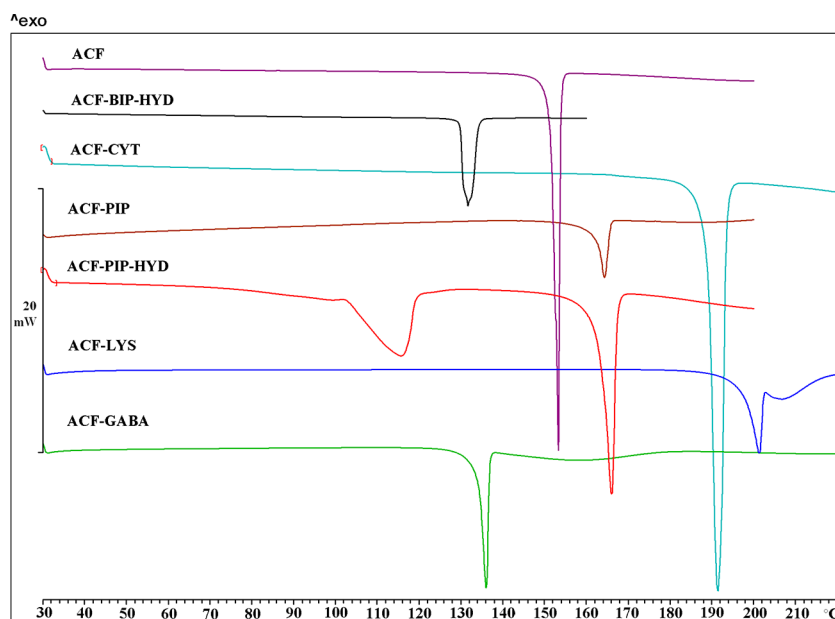


**Figure 7.** DSC heating curves show a sharp melting endotherm for each solid form which is indicative of high purity and homogeneity.

are shown in Figure 8 and the intermediate PXRD patterns are in Figure S9. However, ACF-PIP was found to convert to ACF-PIP-HYD within 3 days (Figure S9f). The crystalline phase stability studies demonstrate good stability of ACF-CYT, ACF-PIP-HYD, ACF-LYS, and ACF-GABA and with the added advantage of higher solubility compared to ACF (solubility curves are discussed later in the paper). We did not

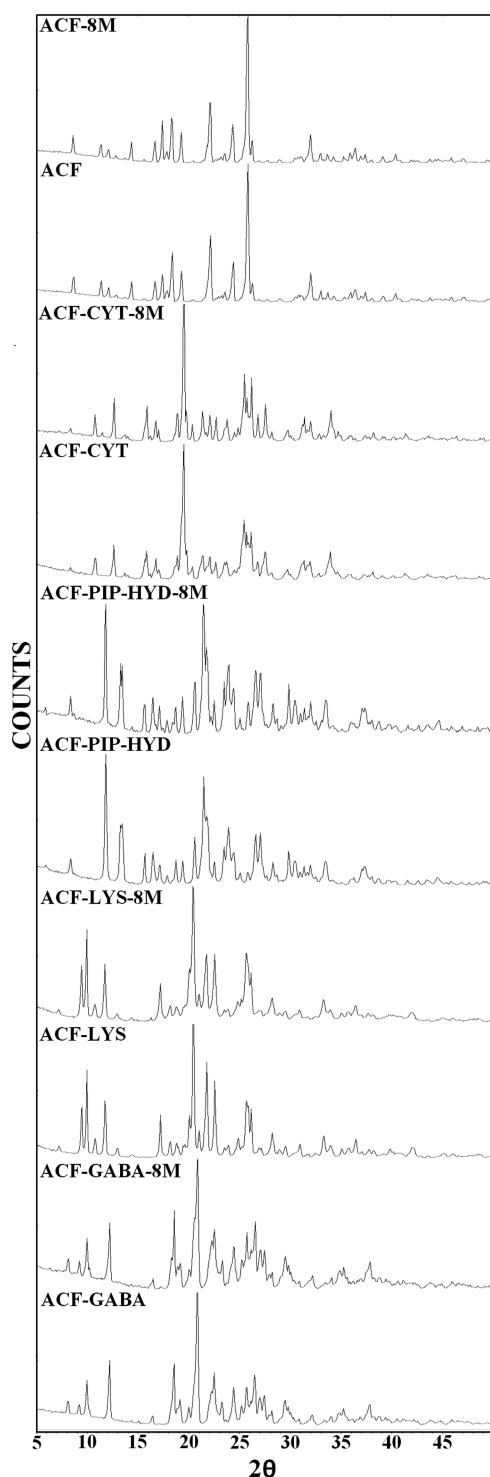


**Figure 8.** Comparison of PXRD plots of salts kept in the stability chamber at 40 °C and 75% RH for 8 months with the PXRD of the starting salts. All salts were stable for up to 8 months except ACF-PIP (shown in Figure S9f).

observe any peaks for byproducts such as diclofenac and/or indolinone shown in Scheme 1 (Figure S9g).

**Crystalline and Amorphous ACF-LYS Salt.** Due to their excess thermodynamic functions, amorphous forms tend to be less stable compared to their crystalline counterparts.<sup>35</sup> The amorphous form of ACF-LYS salt was prepared by lyophilization.<sup>12</sup> The amorphous nature of the product was characterized by PXRD and DSC (Figure S10a,b). PXRD of the amorphous solid kept in accelerated ICH conditions (40 °C, 75% RH) for 24 h matched the crystalline salt (Figure S10c). The same result was observed on slurry grinding of amorphous material in water for 24 h (Figure 9). Stabilization of the amorphous phase is possible, for example, itraconazole as Sporanox beads.<sup>36</sup>

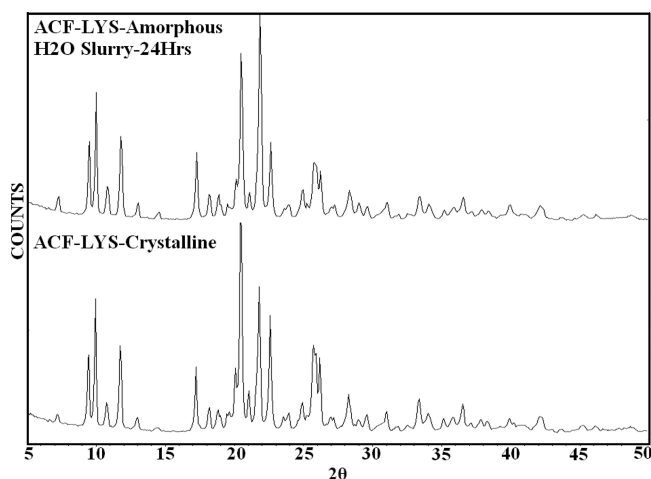


**Figure 9.** PXRD pattern of ACF-LYS amorphous form slurry ground in water for 24 h showed complete conversion to the stable crystalline salt.

**Solubility and Dissolution.** An important goal of drug development is to maintain optimum physicochemical parameters which have a major impact on its efficacy. Solubility and permeability of a drug molecule determine its mode of administration into the body. Solubility remains a major concern for BCS class II drugs since it largely limits bioavailability.<sup>37</sup> Hence, physical or chemical modifications are necessary for such drugs in order to modulate solubility and improve therapeutic efficacy. Solubility and dissolution studies were carried out on ACF (a BCS class II drug) salts to evaluate the solubility advantage. Equilibrium solubility of ACF, ACF-CYT, ACF-PIP-HYD, and ACF-LYS was determined in 25% EtOH-water medium because the concentration of ACF in pure water is very low. The equilibrium solubility experiment was performed for 48 h. Solubility of ACF-PIP and ACF-GABA could not be determined since the former converted to its more stable hydrate and the latter dissociated into the starting components due to the incongruent solubilities of ACF and GABA.<sup>38</sup> The stable ACF-CYT, ACF-PIP-HYD, and ACF-LYS salts exhibited 16.3, 3.5, and 156.5 times higher solubility than the reference drug ACF. PXRD plots of the residue at the end of the equilibrium solubility experiment (Figure S11) confirm that there is no phase transformation or degradation of the salt during the solubility experiment.

Dissolution rate is a time-dependent phenomenon, and this method is preferable for those drugs which undergo phase transformation during the equilibrium solubility experiment.

IDR gives an idea of the peak concentration and the amount of the drug dissolved in a short time period (30 min to 2 h) before it undergoes any phase transformation/dissociation.<sup>39</sup> IDR experiments on ACF salts were performed in 25% EtOH–water for 1.5 h by the rotating disk intrinsic dissolution rate (DIDR) method<sup>40</sup> at 37 °C. ACF–LYS showed 135-fold higher IDR than ACF followed by ACF–GABA ( $\times 112.7$ ), ACF–CYT ( $\times 11.6$ ), ACF–PIP ( $\times 3.4$ ), and ACF–PIP–HYD ( $\times 2.6$ ). As expected, ACF–PIP converted to its hydrate and ACF–GABA dissociated into the starting components in the IDR experiment (Figure S12); the other salts are stable. We did not observe any trend between the melting point of the salt and its dissolution rate; i.e., the lower the melting point, the higher the IDR, similar to those reported for cocrystals.<sup>15a,16a,41</sup> The dissolution rates are better correlated to the coformer solubility (a kinetic parameter) rather than the melting point<sup>42</sup> (thermodynamic). ACF–CYT did not follow this order. Intrinsic dissolution rate curves are displayed in Figure 10, and dissolution rates, melting

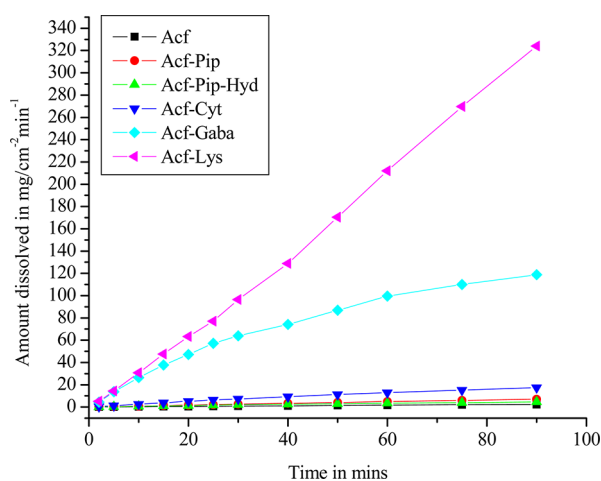


**Figure 10.** Intrinsic dissolution rate curves of ACF salts in 25% EtOH–water.

points, and coformer solubility are listed in Table 5. The amount of dissolved ACF after 1.5 h ( $AUC_{0-1.5}$ ) is 105.33 mg h/L for ACF, 218.5 mg h/L for ACF–PIP–HYD, 836.5 mg h/L for ACF–CYT, and 13451.1 mg h/L for ACF–LYS. The AUC value, which indicates the total dissolved ACF in a given time period, is the highest for ACF–LYS ( $\times 127.7$  times greater than ACF). ACF–LYS salt having the highest dissolution rate and good solid form stability in solubility and humidity experiments is a promising candidate as a soluble ACF salt. Moreover, the salt former L-lysine is completely safe. For

example, ibuprofen lysinate salt is marketed under the brand name Neoprofen.<sup>43</sup>

## CONCLUSIONS

Slurry grinding of ACF with carefully selected GRAS coformers resulted in novel salts of higher solubility, dissolution, and comparable solid form stability. The chemical transformation of ACF to the indolinone derivative under extreme acidic and basic pH was avoided by the use of weak organic bases. A large  $\Delta pK_a$  of  $>6$  resulted in salts with piperazine, lysine, and GABA, and moreover even a small  $\Delta pK_a$  of 2.5 for cytosine also gave a salt. A reason for favorable salt formation with cytosine could be the two-point synthon between 2-aminopyrimidine and COOH group, which facilitates proton transfer. All the salts were characterized by thermal, spectroscopic and diffraction techniques. The stoichiometry of ACF–LYS and ACF–GABA for which single X-ray crystal data could not be obtained was established by <sup>1</sup>H NMR. The intrinsic dissolution rate of ACF–lysine is 135 times, solubility is 156 times, and AUC value is 127 times higher than that of the reference crystalline drug. Solid form stability at accelerated ICH conditions of 40 °C and 75% RH showed that ACF–LYS is stable for over 8 months. The ultimate aim of this work, to improve the solubility of ACF without affecting its solid form stability or cause chemical transformations, was achieved through salt formation using mildly basic coformers. Further physicochemical studies on ACF–LYS salt for drug development are ongoing.

## EXPERIMENTAL SECTION

ACF was obtained from Dalian HongRiDongSheng Import & Export Co. Ltd. (China). Coformers (purity  $> 99.8\%$ ) were purchased from Sigma-Aldrich (Hyderabad, India). Solvents (purity  $> 99\%$ ) were purchased from Hychem Laboratories (Hyderabad, India). Water filtered through a double deionized purification system (Aqua DM, Bhanu, Hyderabad, India) was used for all experiments.

**Preparation of ACF Solid Forms.** ACF (212.4 mg) and 4,4'-BIP (46.8 mg) in a 1:0.5 molar ratio were slurry ground in 5 mL of EtOH for 3 h. The formation of cocrystal hydrate was confirmed by PXRD, DSC, and TGA. Thirty milligrams of this material was dissolved in 5 mL of EtOH and left for slow evaporation at ambient conditions. Single crystals suitable for X-ray diffraction were obtained after 4–5 days.

ACF (212.4 mg) and CYT (66.6 mg) in a 1:1 molar ratio were slurry ground in 5 mL of EtOH for 3 h. Salt formation was confirmed by PXRD. Thirty milligrams of this material was dissolved in 5 mL of EtOH–CH<sub>3</sub>CN 1:1 solvent mixture and left for slow evaporation at ambient conditions. Single crystals suitable for X-ray diffraction were obtained after 4–5 days.

ACF (70.8 mg) and PIP (8.6 mg) in a 1:0.5 molar ratio were dissolved in 5 mL of acetone and left for slow evaporation at ambient conditions. Single crystals suitable for X-ray diffraction were obtained

**Table 5.** Intrinsic Dissolution Rates of ACF Salts along with Their Molar Extinction Coefficient ( $\epsilon$ ), and Melting Point<sup>a</sup>

compound	molar extinction coefficient, $\epsilon$ /mM cm	equilibrium solubility (g/L)	intrinsic dissolution rate, IDR (mg/cm <sup>2</sup> )/min ( $\times 10^{-3}$ )	M.P. (°C)	area under the curve, $AUC_{0-1.5h}$ (mg h)/L	solubility of coformer in water (g/L)
ACF	9.41	0.174	0.022	151.4	105.3	0.058
ACF–CYT	11.61	2.85 ( $\times 16.37$ )	0.256 ( $\times 11.64$ )	185.2	836.5 ( $\times 7.9$ )	7.7
ACF–PIP	8.33		0.076 ( $\times 3.46$ )	164.2	316.3 ( $\times 3.0$ )	1000
ACF–PIP–HYD	9.57	1.01 ( $\times 3.56$ )	0.057 ( $\times 2.59$ )	162.4	218.5 ( $\times 2.1$ )	1000
ACF–LYS	9.26	27.23 ( $\times 156.51$ )	2.97 ( $\times 135.0$ )	201.0	13451.1 ( $\times 127.7$ )	1500
ACF–GABA	10.28		2.48 ( $\times 112.7$ )	135.5	6431.1 ( $\times 61.1$ )	1300

<sup>a</sup>The number of times enhancement of IDR and AUC with respect to ACF is given in parentheses.

after 4 h. The starting materials were crystallized in above conditions repeatedly to obtain the bulk material.

ACF (70.8 mg) and PIP (8.6 mg) in a 1:0.5 molar ratio were slurry ground in 5 mL of EtOH for 3 h. The salt hydrate was formed based on PXRD, DSC, and TGA. Thirty milligrams of this material was dissolved in 5 mL of EtOH–CH<sub>3</sub>CN 1:1 solvent mixture and left for slow evaporation at ambient conditions. Single crystals suitable for X-ray diffraction were obtained after 4–5 days.

ACF (212.4 mg) and LYS (87.6 mg) in a 1:1 molar ratio were slurry ground in 5 mL of EtOH for 3 h. Salt formation was confirmed by PXRD and <sup>1</sup>H NMR.

ACF (212.4 mg) and GABA (61.8 mg) in a 1:1 molar ratio were slurry ground in 5 mL of EtOH for 3 h. Salt formation was confirmed by PXRD and <sup>1</sup>H NMR.

To a solution of 292 mg of LYS in 20 mL of water, 708 mg of ACF was added with stirring. The solution was filtered through Whatmann filter paper and lyophilized. The ACF–LYS salt residue was obtained as an amorphous powder.

**<sup>1</sup>H NMR Spectroscopy.** All ground products were characterized by <sup>1</sup>H NMR to confirm their stoichiometry (Figure S6). Proton NMR spectra were recorded on Bruker Avance 400 MHz spectrometer (Bruker-Biospin, Karlsruhe, Germany). Chemical shifts are quoted in  $\delta$  scale and *J* coupling in Hz.

ACF–LYS (1:1). <sup>1</sup>H NMR (D<sub>2</sub>O): 1.28 (2H, quintet, *J* 7.5), 1.51 (2H, quintet, *J* 7.5), 1.68 (2H, q, *J* 7.5), 2.78 (2H, t, *J* 7.5), 3.79 (2H, s), 4.28 (2H, s), 6.21 (1H, d, *J* 8), 6.83 (1H, t, *J* 8), 7.0 (1H, t, *J* 8), 7.11 (1H, t, *J* 8), 7.19 (1H, d, *J* 8), 7.39 (2H, d, *J* 8). COOHs and NHs of ACF and LYS exchange in solvent.

ACF–GABA (1:1). <sup>1</sup>H NMR (DMSO-*d*<sub>6</sub>): 1.70 (2H, quintet, *J* 7.5), 2.27 (2H, t, *J* 7.5), 2.74 (2H, t, *J* 7.5), 3.81 (2H, s), 4.33 (2H, s), 6.22 (1H, d, *J* 8), 6.83 (1H, t, *J* 8), 7.0 (1H, t, *J* 8), 7.18 (1H, t, *J* 8), 7.20 (1H, d, *J* 8), 7.49 (2H, d, *J* 8). COOHs and NHs of ACF and GABA exchange in solvent.

**Vibrational Spectroscopy.** Thermo-Nicolet 6700 Fourier transform infrared spectrophotometer with NXR-Fourier transform Raman module (Thermo Scientific, Waltham, Massachusetts) was used to record IR and Raman spectra. IR was recorded on sample dispersed in KBr pellet. Raman spectra were recorded on sample contained in standard NMR diameter tube or on compressed sample contained in a gold-coated sample holder. Data were analyzed using the Omnic software (Thermo Scientific, Waltham, Massachusetts).

**Solid-State NMR Spectroscopy.** Solid-state <sup>13</sup>C NMR spectra were recorded on Bruker Avance 400 MHz spectrometer (Bruker-Biospin, Karlsruhe, Germany, operating at 100 MHz for <sup>13</sup>C nucleus). ss-NMR measurements were carried out on Bruker 4-mm double resonance CP-MAS probe in zirconia rotors with a Kel-F cap at 5.0 kHz spinning rate with a cross-polarization contact time of 2.5 ms and a delay of 8 s. <sup>13</sup>C NMR spectra were recorded at 100 MHz and referenced to the methylene carbon of glycine, and then recalibrated to the TMS scale ( $\delta_{\text{glycine}} = 43.3$  ppm).

**Thermal Analysis.** DSC was performed on a Mettler-Toledo DSC 822e module, and thermogravimetric analysis (TGA) was performed on a Mettler Toledo TGA/SDTA 851e module (Mettler-Toledo, Columbus, Ohio). Samples were placed in sealed pin-pricked alumina pans for TG experiments and in crimped but vented aluminum pans for DSC experiments. The typical sample size is 3–5 mg for DSC and 8–12 mg for TGA. The temperature range for the heating curve was 30–220 °C, and the sample was heated at a rate of 5 °C/min. Samples were purged in a stream of dry nitrogen flowing at 80 mL/min for DSC and 50 mL/min for TGA.

**Powder X-ray Diffraction.** PXRD of all the samples was recorded on Bruker D8 Advance diffractometer (Bruker-AXS, Karlsruhe, Germany) using Cu–K $\alpha$  X-radiation ( $\lambda = 1.5406$  Å) at 40 kV and 30 mA power. XRD patterns were collected over the  $2\theta$  range 5–50° at a scan rate of 1°/min. Powder Cell 2.4<sup>44</sup> (Federal Institute of Materials Research and Testing, Berlin, Germany) was used for Rietveld refinement of experimental PXRD and calculated lines from the X-ray crystal structure.

**X-ray Crystallography.** X-ray reflections were collected on Bruker SMART-APEX CCD diffractometer (Bruker-AXS, Karlsruhe, Ger-

many). Mo–K $\alpha$  X-radiation ( $\lambda = 0.71073$  Å) was used to collect X-ray reflections on the single crystal at 100 K. Data reduction was performed using the Bruker SAINT software.<sup>45</sup> Intensities for absorption were corrected using SADABS,<sup>46</sup> the Siemens area detector absorption correction program (Bruker-AXS). Crystal structures were solved and refined using SHELX-97<sup>47</sup> with anisotropic displacement parameters for non-H atoms. Hydrogen atoms on O and N were experimentally located in difference electron density maps. All C–H atoms were fixed geometrically using HFIX command in SHELX-TL (Bruker-AXS). The stoichiometry of water molecule in ACF–BIP–H<sub>2</sub>O was fixed to 0.5 s.o.f. and hydrogens attached to it were fixed using the DFIX command. A check of the final CIF file using PLATON<sup>48</sup> did not show any missed symmetry. Hydrogen bond distances shown in Table 3 are neutron normalized to fix the D–H distance to its accurate neutron value in the X-ray crystal structures (O–H 0.983 Å, N–H 1.009 Å, and C–H 1.083 Å). X-Seed<sup>49</sup> was used to prepare packing diagrams. Crystallographic .cif files (CCDC Nos. 915223–915227) are available at www.ccdc.cam.ac.uk/data or as part of Supporting Information.

**Solid Form Stability.** About 200 mg of each solid compounds was placed in an open Petri dish and stored without a lid in a Thermolab T-908 stability chamber (Thermolab Instruments, Mumbai, India) premainained at 40 °C and 75% RH (as per the WHO/ICH guidelines) for 8 months. Solid form stability and integrity of the samples were assessed periodically every week by PXRD.

**Dissolution and Solubility Measurements.** The solubility curves of ACF salts were measured using the Higuchi and Connor method<sup>50</sup> in 25% ethanol–water medium at 30 °C. First, the absorbance of a known concentration of the salt was measured at the given  $\lambda_{\text{max}}$  (ACF 274 nm, ACF–CYT 270 nm, ACF–PIP 273 nm, ACF–PIP–HYD 273 nm, ACF–LYS 275 nm, ACF–GABA 274 nm) in 25% ethanol–water on Thermo Scientific Evolution 300 UV–vis spectrometer (Thermo Scientific, Waltham, MA). These absorbance values were plotted against several known concentrations to prepare the concentration versus intensity calibration curve. From the slope of the calibration curves, molar extinction coefficients for ACF salts were calculated. An excess amount of the sample was added to 6 mL of 25% ethanol–water. The supersaturated solution was stirred at 300 rpm using a magnetic stirrer at 30 °C. After 24 h, the suspension was filtered through Whatman's 0.45  $\mu\text{m}$  syringe filter. The filtered aliquots were diluted sufficiently, and the absorbance was measured at the given  $\lambda_{\text{max}}$ . IDR experiments were carried out on USP-certified Electrolab TDT-08L dissolution tester (Mumbai, India). Dissolution experiments were performed for 1.5 h in 25% ethanol–water at 37 °C. Prior to IDR estimation, standard curves for all the compounds were obtained spectrophotometrically at their respective  $\lambda_{\text{max}}$ . The calculated molar extinction coefficients were used to determine the IDR values. For IDR measurements, 200 mg of the compound was taken in the intrinsic attachment and compressed to a 0.5-cm<sup>2</sup> disk using a hydraulic press 4.0 ton/in.<sup>2</sup> pressure for 5 min. The intrinsic attachment was placed in a jar of 500 mL of medium preheated to 37 °C and rotated at 150 rpm. Five milliliters of the aliquot was collected at specific time intervals, and the concentration of the aliquots was determined with appropriate dilutions from the predetermined standard curves of the respective compounds. The IDR of the compound was calculated in the linear region of the dissolution curve (which is the slope of the curve or amount of drug dissolved/surface area of the disk) per unit time. The identity of the undissolved material after the dissolution experiment was ascertained by PXRD. The nature of the solid samples after disk compression and solubility/dissolution measurements was verified by PXRD.

## ■ ASSOCIATED CONTENT

### Supporting Information

Crystallographic information (.cif files); ORTEP of indolinone (Figure S1); <sup>1</sup>H NMR spectra of ACF–LYS and ACF–GABA (Figure S2); ORTEP of ACF, ACF–BIP–H<sub>2</sub>O (1:0.5:0.5), ACF–CYT (1:1), ACF–PIP (1:0.5), ACF–PIP–H<sub>2</sub>O (1:0.5:1) (Figure S3); powder XRD patterns of all solid forms (Figure

S4), DSC, TGA, and HSM of ACF–BIP–HYD, ACF–PIP–HYD (Figure S5); IR spectra of all solid forms (Figure S6); Raman spectra of all solid forms (Figure S7); ss-NMR spectra of all solid forms (Figure S8); 6 months accelerated stability experiments of all solid forms (Figure S9); DSC and PXRD comparisons of ACF–LYS amorphous and crystalline salt and PXRD comparison of amorphous to crystalline ACF–LYS salt conversion in humidity experiments (Figure S10); PXRD of ACF, ACF–CYT, ACF–PIP–HYD, ACF–PIP, ACF–LYS, ACF–GABA at 24 h of slurry experiment (Figure S11); PXRD of ACF–PIP and ACF–GABA at 90 min of dissolution experiment (Figure S12); torsion angles of all solid forms (Table S1), IR vibrational frequencies of ACF and salts (Table S2); Raman vibrational frequencies of ACF and salts (Table S3); and  $^{13}\text{C}$  ss-NMR chemical shifts of ACF and salts (Table S4). This material is available free of charge via the Internet at <http://pubs.acs.org>.

## AUTHOR INFORMATION

### Corresponding Author

\*E-mail: [ashwini.nangia@gmail.com](mailto:ashwini.nangia@gmail.com).

### Notes

The authors declare no competing financial interest.

## ACKNOWLEDGMENTS

N.R.G. and K.S. thank CSIR and UGC for a fellowship. We thank the Department of Science and Technology (J.C. Bose fellowship SR/S2/JCB-06/2009) and Council of Scientific and Industrial Research (Pharmaceutical Cocrystals Project 01/2410/10/EMR-II) for funding. DST (IRPHA) and University Grants Commission (UGC-PURSE grant) are thanked for providing instrumentation and infrastructure facilities at University of Hyderabad (UOH).

## REFERENCES

- (1) Huang, L. F.; Tong, W. Q. *Adv. Drug Delivery Rev.* **2004**, *56*, 321–334.
- (2) (a) Goud, N. R.; Gangavaram, S.; Suresh, K.; Pal, S.; Manjunatha, S. G.; Nambiar, S.; Nangia, A. *J. Pharm. Sci.* **2012**, *101*, 664. (b) Babu, N. J.; Nangia, A. *Cryst. Growth Des.* **2011**, *11*, 2662. (c) Blagden, N.; de Matas, M.; Gavan, P. T.; York, P. *Adv. Drug Delivery Rev.* **2007**, *59*, 617.
- (3) (a) Berge, S. M.; Bighley, L. D.; Monkhouse, D. C. *J. Pharm. Sci.* **1977**, *66*, 1. (b) Sweetana, S.; Akers, M. J. *J. Pharm. Sci. Tech.* **1996**, *50*, 330.
- (4) (a) Thayer, A. M. *Chem. Eng. News* **2013**, *91*, 10. (b) Babu, N. J.; Sanphui, P.; Nangia, A. *Chem. Asian J.* **2012**, *7*, 2274. (c) Yan, Y.; Chen, J. M.; Geng, N.; Lu, T. B. *Cryst. Growth Des.* **2012**, *12*, 2226. (d) Sanphui, P.; Kumar, S. S.; Nangia, A. *Cryst. Growth Des.* **2012**, *12*, 4588.
- (5) (a) British Pharmacopoeia, The Stationary Office, MHRA, British Pharmacopoeial Commission Office, London, 2005. (b) Reynolds, J. E. F. *Martindale: The Complete Drug Reference*; Pharmaceutical Press: London, 1999.
- (6) (a) Lee, B.; Jung, H. *Pharm. Sci. Suppl.* **1999**, *4*, 14. (b) Kim, T.; Shin, J.; Lee, B. *AAPS Annual Meeting, Denver, Colorado*, 2001.
- (7) Sevukarajan, M.; Parveen, S. S.; Nair, R.; Badivaddin, T. M. *J. Pharm. Sci. Res.* **2011**, *3*, 1280.
- (8) Kim, N. W.; Il, J. Novel Amino acid Salt of Aceclofenac having high bioavailability and Pharmaceutical preparation comprising the same as Active Ingredient. Patent No. 1020050005894A, Korean Industrial Property Office, Korea, 2003.
- (9) (a) Maulvi, F. A.; Dalwadi, S. J.; Thakkar, V. T.; Soni, T. G.; Gohel, M. C.; Gandhi, T. R. *Powder Technol.* **2011**, *207*, 47. (b) Shinde, S. S.; Patil, S. S.; Mevekari, F. I.; Satpute, A. S. *Int. J. Adv. Pharm. Sci.* **2010**, *1*, 299.
- (10) Sevukarajan, M.; Thanuja, B.; Riyaz, S.; Rahul, N. *J. Pharm. Sci. Res.* **2011**, *3*, 1288.
- (11) Casas, A. V.; Rue du, R. New 2-((2,6-dichlorophenyl)amine)-phenylacetoxyacetyl derivatives, the process for preparing the same and their use in therapeutics. Patent No. EP0119932A1, European Patent Office, Barcelona, 1984.
- (12) Sallmann, A. New Salts of 2-[(2,6-dichlorophenyl)amine]-phenylacetoxyacetic acid with organic basic cations. Patent No. US005708024A, United States patent office, 1998.
- (13) Azhlawar, S.; Ravi, T. K. *Int. J. Pharm. Pharm. Sci.* **2011**, *3*, 245.
- (14) (a) Desiraju, G. R.; Vittal, J. J.; Ramanan, A. *Crystal Engineering, A Textbook*; World Scientific Publishing: Singapore, 2011. (b) Desiraju, G. R. *Crystal Engineering. The Design of Organic Solids*; Elsevier: Amsterdam, 1989.
- (15) (a) Schultheiss, N.; Newman, A. *Cryst. Growth Des.* **2009**, *9*, 2950. (b) Jones, W.; Motherwell, W. D. S.; Trask, A. V. *MRS Bull.* **2006**, *31*, 875. (c) Almarsson, Ö.; Zaworotko, M. J. *Chem. Commun.* **2004**, *17*, 1889.
- (16) (a) Stanton, M. K.; Bak, A. *Cryst. Growth Des.* **2008**, *8*, 3856. (b) Stanton, M. K.; Tufekcic, S.; Morgan, C.; Bak, A. *Cryst. Growth Des.* **2009**, *9*, 1344. (c) Bak, A.; Gore, A.; Yanez, E.; Stanton, M.; Tufekcic, S.; Syed, R.; Akrami, A.; Rose, M.; Surapaneni, S.; Bostick, T.; King, A.; Neervannan, S.; Ostovic, D.; Koparkar, A. *J. Pharm. Sci.* **2008**, *97*, 3942.
- (17) (a) Desiraju, G. R. *Angew. Chem., Int. Ed. Engl.* **1995**, *34*, 2311. (b) Walsh, R. D. B.; Bradner, M. W.; Fleischman, S.; Morales, L. A.; Moulton, B.; Rodríguez-Hornedo, N.; Zaworotko, M. J. *Chem. Commun.* **2003**, 186.
- (18) (a) Trask, A. V.; Jones, W. *Top. Curr. Chem.* **2005**, *254*, 41. (b) Shan, N.; Toda, F.; Jones, W. *Chem. Commun.* **2002**, *20*, 2372.
- (19) GRAS chemicals list may be accessed at [www.fda.gov/Food/FoodIngredientsPackaging/GenerallyRecognizeasSafeGRAS/GRASSubstancesSCOGSDatabase/default.htm](http://www.fda.gov/Food/FoodIngredientsPackaging/GenerallyRecognizeasSafeGRAS/GRASSubstancesSCOGSDatabase/default.htm).
- (20) (a) Aakeroy, C. B.; Fasulo, M. E.; Desper, J. *Mol. Pharmaceutics* **2007**, *4*, 317. (b) Sarma, B.; Nath, N. K.; Bhogala, B. R.; Nangia, A. *Cryst. Growth Des.* **2009**, *9*, 1546. (c) Childs, S. L.; Stahly, G. P.; Park, A. *Mol. Pharmaceutics* **2007**, *4*, 323. (d) Cruz-Cabeza, A. J. *CrystEngComm* **2012**, *14*, 6362.
- (21) Alvarez-Larena, A.; Piniella, J. F.; Carrasco, E.; Ginebreda, A.; Julia, S.; Germain, G. *J. Crystallogr. Spec. Res.* **1992**, *22*, 323.
- (22) Perlovich, G. L.; Surov, A. O.; Hansen, L. K.; Bauer-Brandl, A. *J. Pharm. Sci.* **2007**, *96*, 1031.
- (23) (a) Chen, X.; Morris, K. R.; Griesser, U. J.; Byrn, S. R.; Stowell, J. G. *J. Am. Chem. Soc.* **2002**, *124*, 15012. (b) Cox, P. J.; Manson, P. L. *Acta Crystallogr.* **2003**, *E59*, 986.
- (24) (a) Kuduva, S. S.; Craig, D. C.; Nangia, A.; Desiraju, G. R. *J. Am. Chem. Soc.* **1999**, *121*, 1936. (b) Das, D.; Jetti, R. K. R.; Boese, R.; Desiraju, G. R. *Cryst. Growth Des.* **2003**, *3*, 675. (c) Das, D.; Desiraju, G. R. *Chem. – Asian J.* **2006**, *1*, 231.
- (25) (a) Bernstein, J.; Davis, R. E.; Shimoni, L.; Chang, N. L. *Angew. Chem., Int. Ed. Engl.* **1995**, *34*, 1555. (b) Etter, M. C. *Acc. Chem. Res.* **1990**, *23*, 120. (c) Etter, M. C. *J. Phys. Chem.* **1991**, *95*, 4601.
- (26) Sanphui, P.; Bolla, G.; Das, U.; Mukherjee, A. K.; Nangia, A. *CrystEngComm* **2013**, *15*, 34.
- (27) (a) Etter, M. C.; Macdonald, J. C.; Bernstein, J. *Acta Crystallogr.* **1990**, *B46*, 256. (b) Etter, M. C.; Reutzel, S. M. *J. Am. Chem. Soc.* **1991**, *113*, 2586.
- (28) (a) Stevens, J. S.; Byard, S. J.; Schroeder, S. L. M. *J. Pharm. Sci.* **2010**, *99*, 4453. (b) Li, Z. J.; Abramov, Y.; Bordner, J.; Leonard, J.; Medek, A.; Trask, A. V. *J. Am. Chem. Soc.* **2006**, *128*, 8199.
- (29) Sanphui, P.; Bolla, G.; Nangia, A. *Cryst. Growth Des.* **2012**, *12*, 2023.
- (30) (a) Nangia, A. *Acc. Chem. Res.* **2008**, *41*, 595. (b) Babu, N. J.; Cherukuvada, S.; Thakuria, R.; Nangia, A. *Cryst. Growth Des.* **2010**, *10*, 1979.
- (31) (a) Remenar, J. F.; Peterson, M. L.; Stephens, P. W.; Zhang, Z.; Zimekov, Y.; Hickey, M. B. *Mol. Pharmaceutics* **2007**, *4*, 386. (b) Karki,

S.; Friščić, T.; Fábíán, L.; Jones, W. *CrystEngComm* **2010**, *12*, 4038.  
(c) André, V.; Fernandes, A.; Santos, P. P.; Duarte, M. T. *Cryst. Growth Des.* **2011**, *11*, 2325.

(32) (a) Silverstein, R. M. *Spectrometric Identification of Organic Compounds*, 6th ed.; John Wiley & Sons, Inc.: New York, 2002.  
(b) Smith, E.; Dent, G. *Modern Raman Spectroscopy, A Practical Approach*; John Wiley: New York, 2005.

(33) (a) Vogt, F. G.; Clawson, J. S.; Strohmeier, M.; Edwards, A. J.; Pham, T. N.; Watson, S. A. *Cryst. Growth Des.* **2009**, *9*, 921. (b) Braga, D.; Maini, L.; de Sanctis, G.; Rubini, K.; Grepioni, F.; Chierotti, M. R.; Gobetto, R. *Chem—Eur. J.* **2003**, *9*, 5538.

(34) Stability testing of Active Pharmaceutical Ingredients and Finished Pharmaceutical Products, WHO Technical Report Series, No. 953, [http://www.ich.org/fileadmin/Public\\_Web\\_Site/ICH\\_Products/Guidelines/Quality/Q1F/Stability\\_Guideline\\_WHO.pdf](http://www.ich.org/fileadmin/Public_Web_Site/ICH_Products/Guidelines/Quality/Q1F/Stability_Guideline_WHO.pdf)

(35) (a) Hancock, B. C.; Zograf, G. J. *Pharm. Sci.* **1997**, *86*, 1.  
(b) Craig, D. Q. M.; Royall, P. G.; Kett, V. L.; Hopton, M. L. *Int. J. Pharm.* **1999**, *179*, 179. (c) Singhal, D.; Curatolo, W. *Adv. Drug Delivery Rev.* **2004**, *56*, 335.

(36) Sporanox capsules (made by Janssen Pharmaceutica) contain amorphous itraconazole coated on 0.4–0.5 mm diameter sucrose spheres. Other inactive ingredients include hydroxypropyl methylcellulose, poly(ethyleneglycol) (PEG) 20 000, and starch.

(37) (a) Takagi, T.; Ramachandran, C.; Bermejo, M.; Yamashita, S.; Yu, L. X.; Amidon, G. L. *Mol. Pharmaceutics* **2006**, *3*, 631. (b) Lipinski, C. A. Solubility in Water and DMSO: issues and potential Solutions. In *Pharmaceutical Profiling in Drug Discovery for Lead Selection*: Borchardt, R. T.; Kerns, E. H.; Lipinski, C. A.; Thakker, D. R.; Wang, B., Eds.; AAPS Press: Arlington, VA, 2004; pp 93–125.

(38) Childs, S. L.; Rodríguez-Hornedo, N.; Reddy, L. S.; Jayasankar, A.; Maheshwari, C.; McCausland, L.; Shipplett, R.; Stahly, B. C. *CrystEngComm* **2008**, *10*, 856.

(39) Dressman, J. B.; Amidon, G. L.; Reppas, C.; Shah, V. P. *Pharm. Res.* **1998**, *15*, 11.

(40) Yu, L. X.; Carlin, A. S.; Amidon, G. L.; Hussain, A. S. *Int. J. Pharm.* **2004**, *270*, 221.

(41) Abramowitz, R.; Yalkowsky, S. H. *Pharm. Res.* **1990**, *7*, 942.

(42) Good, D. J.; Rodríguez-Hornedo, N. *Cryst. Growth Des.* **2009**, *9*, 2252.

(43) (a) Su, P. H.; Chen, J. Y.; Su, C. M.; Huang, T. C.; Lee, H. S. *Pediatr. Int.* **2003**, *45*, 665. (b) Geisslinger, G.; Dietzel, K.; Bezler, H.; Nuernberg, B.; Brune, K. *Int. J. Clin. Pharmacol. Ther. Toxicol.* **1989**, *27*, 324.

(44) Powder Cell, a program for structure visualization, powder pattern calculation and profile fitting. <http://www.ccp14.ac.uk/tutorial/powdcell/>.

(45) *SAINTE-Plus*, Ver. 6.45; Bruker AXS: Madison, WI, 2003.

(46) Sheldrick, G. M. *SADABS, Program for Empirical Absorption Correction of Area Detector Data*; University of Göttingen: Göttingen, Germany, 1997.

(47) Sheldrick, G. M. *SHELX-97, Program for the Solution and Refinement of Crystal Structures*; University of Göttingen: Göttingen, Germany, 1997.

(48) Spek, A. L. *PLATON: A Multipurpose Crystallographic Tool*; Utrecht University: Utrecht, The Netherlands, 2002. Spek, A. L. *J. Appl. Crystallogr.* **2003**, *36*, 7.

(49) (a) Barbour, L. J. *Supramol. Chem.* **2001**, *1*, 189. (b) Barbour, L. J. *X-Seed, Graphical Interface to SHELX-97 and POV-Ray*; University of Missouri–Columbia: Columbus, MO, 1999.

(50) Higuchi, T.; Connors, K. A. *Adv. Anal. Chem. Instrum.* **1965**, *4*, 117.